

Fragment-Based Discovery of Subtype-Selective Adenosine Receptor Ligands from Homology Models

Anirudh Ranganathan,^{†,||} Leigh A. Stoddart,^{‡,||} Stephen J. Hill,^{*,‡} and Jens Carlsson^{*,§}

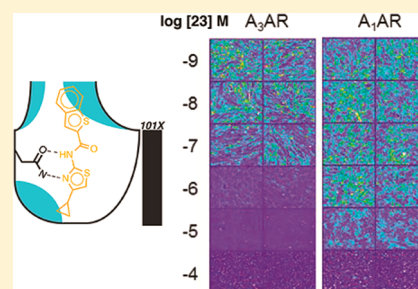
[†]Science for Life Laboratory, Department of Biochemistry and Biophysics, and Center for Biomembrane Research, Stockholm University, SE-106 91 Stockholm, Sweden

[‡]Cell Signalling Research Group, School of Life Sciences, University of Nottingham, Nottingham NG7 2UH, U.K.

[§]Science for Life Laboratory, Department of Medicinal Chemistry, BMC, Uppsala University, P.O. Box 574, SE-751 23 Uppsala, Sweden

S Supporting Information

ABSTRACT: Fragment-based lead discovery (FBLD) holds great promise for drug discovery, but applications to G protein-coupled receptors (GPCRs) have been limited by a lack of sensitive screening techniques and scarce structural information. If virtual screening against homology models of GPCRs could be used to identify fragment ligands, FBLD could be extended to numerous important drug targets and contribute to efficient lead generation. Access to models of multiple receptors may further enable the discovery of fragments that bind specifically to the desired target. To investigate these questions, we used molecular docking to screen >500 000 fragments against homology models of the A₃ and A₁ adenosine receptors (ARs) with the goal to discover A₃AR-selective ligands. Twenty-one fragments with predicted A₃AR-specific binding were evaluated in live-cell fluorescence-based assays; of eight verified ligands, six displayed A₃/A₁ selectivity, and three of these had high affinities ranging from 0.1 to 1.3 μM. Subsequently, structure-guided fragment-to-lead optimization led to the identification of a >100-fold-selective antagonist with nanomolar affinity from commercial libraries. These results highlight that molecular docking screening can guide fragment-based discovery of selective ligands even if the structures of both the target and antitarget receptors are unknown. The same approach can be readily extended to a large number of pharmaceutically important targets.



■ INTRODUCTION

Fragment-based lead discovery (FBLD) has rapidly developed into one of the main strategies for early-phase drug development. Drug discovery programs driven by FBLD have quickly progressed into clinical trials, and fragment screens have been applied successfully to targets for which high-throughput screening (HTS) approaches have failed.¹ The main difference between HTS and FBLD is that the latter approach initially focuses on the identification of ligands that are less than half the size of a drug. Because of the lower complexity of fragments compared with drug-like molecules, screens of chemical libraries with hundreds to thousands of compounds cover sufficient portions of chemical space to identify ligands. This makes FBLD an attractive alternative to HTS, which may require screening of libraries that are several orders of magnitude larger to identify lead compounds.¹ As fragments are typically low-affinity ligands, a major challenge in FBLD has been the development of sensitive screening techniques. This has been particularly problematic for membrane proteins, which include important drug targets such as G protein-coupled receptors (GPCRs) and ion channels.² Recently, fragment screens using NMR-,³ surface plasmon resonance (SPR)-,⁴ and fluorescence-based⁵ methods have successfully been applied to GPCRs, making it feasible to begin utilizing FBLD for the large number of important drug targets in this superfamily.⁶

The weakly binding ligands that emerge from fragment screens occupy subpockets on the protein surface and have to be combined or grown to generate potent lead compounds.⁷ Fragments typically lack specificity because of their low molecular complexity,⁸ which makes it a challenge to achieve selectivity for the desired target.⁹ The identification of selective lead compounds is of particular importance for GPCRs, as many subtypes recognize the same ligands, resulting in orthosteric binding sites with a high degree of homology. For many soluble targets, FBLD can often take advantage of the relative ease of generating crystal structures for protein–fragment complexes, which can provide invaluable information in ligand optimization.¹⁰ Recent breakthroughs in this area have resulted in atomic-resolution crystal structures for GPCRs,¹¹ and in a few cases it has even been feasible to resolve the binding modes of fragment ligands.¹² On the basis of the detailed information provided by crystal structures, virtual screening has been used successfully to discover fragment ligands with high hit rates for soluble proteins^{9,13} and, more recently, GPCRs.^{14,15} However, as the determination of GPCR crystal structures still requires considerable experimental effort, *in silico* fragment screening remains limited to the small

Received: July 16, 2015

Published: November 22, 2015

number of crystallized targets. On the other hand, if homology models based on available templates could be utilized in FBLD, structure-guided discovery and optimization of fragments could be applied to a large fraction of the GPCR superfamily, but this has rarely been attempted.^{16,17} Moreover, access to models of several receptor subtypes may also enable the efficient design of selective leads, which is crucial in drug development to avoid adverse effects caused by interactions with unintended targets.

In this work, we explored the prospect of using *in silico* screening of commercially available libraries to identify and optimize subtype-selective fragments targeting GPCRs of unknown structure. The target GPCR, the A₃ adenosine receptor (A₃AR), belongs to a family of four human receptors that recognize adenosine and was selected for its potential as a drug target for a wide range of diseases, including glaucoma (antagonists), cancer (agonists), and asthma (antagonists).^{18,19} As interactions with the closely related A₁ adenosine receptor (A₁AR) may cause cardiac complications²⁰ (A₁ agonists) and lead to increased risks for seizure and stroke (A₁ antagonists),¹⁹ fragments that selectively bind to the A₃AR over the A₁AR were sought. We generated models of the A₃AR and A₁AR based on a crystal structure of the A_{2A}AR and carried out molecular docking screens of >0.5 million fragments against both receptors. Fragments predicted to bind preferentially to the A₃AR over the A₁AR were evaluated in a live-cell fluorescence-based high-content screening assay. To further probe the utility of our approach, the A₁- and A₃AR homology models were also used to guide the optimization of fragment potency and selectivity. On the basis of our results, the feasibility of structure-guided FBLD for GPCRs of unknown structure will be discussed.

RESULTS

Homology Modeling of the A₃ and A₁ Adenosine Receptors. As no crystal structures of the A₃- and A₁AR were available, protocols for the generation of homology models for the target and antitarget receptors were developed. A structure of the A₃AR binding site was required in order to predict ligands, and modeling of the A₁AR was essential for assessing the selectivity by comparing differences between the predicted binding energies from molecular docking for the two subtypes. The protocol for optimization of the homology models is summarized in Figure 1.

Homology modeling of the A₃- and A₁AR was based on a high-resolution crystal structure of the closely related A_{2A}AR,²¹ which has 51% and 59% sequence identity to the A₃- and A₁AR, respectively, in the transmembrane region (Figure S1). To identify a suitable model of the A₃AR, a ligand-guided homology modeling approach was employed.^{22,23} Initially, 1000 A₃AR homology models were generated, and the 300 structures with the highest model quality, as judged by their DOPE scores,²⁴ were further evaluated. Docking screens of two sets of compounds were used to assess the ability of the A₃AR models to recognize known ligands. One set of lead-like ligands and one set of >50-fold subtype-selective A₃AR ligands were compiled, and 50 decoys per ligand were added to each compound set.²⁵ The lead-like set was first docked to the 300 A₃AR homology models using DOCK3.6.²⁶ The ability of a model to enrich ligands over decoys was assessed on the basis of a receiver operator characteristic (ROC) curve and quantified using the adjusted logarithm of area under the curve (aLogAUC) metric.²⁷ A positive aLogAUC value for a given model indicates that enrichment of ligands over decoys is

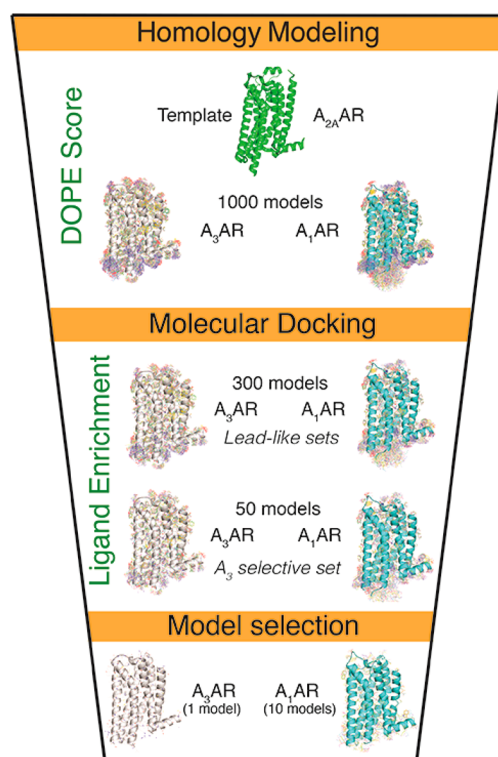


Figure 1. Summary of the modeling protocol for the A₃- and A₁AR. Ligand-guided homology modeling was used to identify homology models suitable for virtual screening. In a first step, 1000 homology models for each receptor based on an A_{2A}AR crystal structure were generated. Docking screens against the 300 homology models with the best model quality scores were then used to identify 50 binding site structures of the A₃- and A₁AR with the ability to recognize known (lead-like) ligands. Molecular docking of A₃AR-selective ligands to the 50 models was used to guide the selection of a single structure for the A₃AR subtype and an ensemble of 10 A₁AR structures, which were used in the prospective screens. The A₁-, A_{2A}-, and A₃AR are depicted in cyan, green, and white, respectively.

better than random. The 50 models with the best aLogAUC values, ranging from 31 to 39, were taken forward for further assessment (Figures 1 and S2a). These binding site models displayed strong enrichment of known ligands and ranked them 26-fold better than expected from random selection in the top 1% of the screened database. The set of A₃AR-selective ligands together with decoys was then docked to the 50 remaining models. The ligand enrichments for these models were again significantly better than random (aLogAUC = 11–41). The homology model with the best enrichment of lead-like and A₃AR-selective compounds was also judged to produce binding modes that agreed with those observed for ligands in available crystal structures of the A_{2A}AR²¹ (Figure 2a), and this model was taken forward for prospective screening.

As in the case of the A₃AR, 1000 homology models were also generated for the A₁AR, and retrospective screens of lead-like ligands along with decoys against 300 structures were carried out to identify suitable binding site structures. The resulting enrichments were again significantly better than random for a majority of the models (Figure S2b). The A₃AR-selective ligand set was then docked to the 50 best models. However, in contrast to the A₃AR modeling protocol, the goal was to identify A₁AR structures that did not enrich these compounds to bias the prospective docking screen toward the discovery of

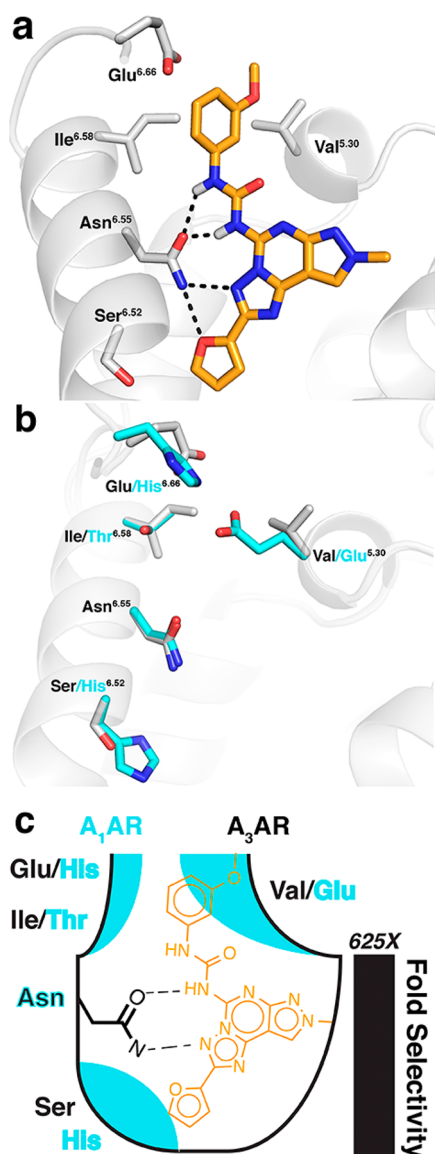


Figure 2. Structural basis of subtype selectivity. (a) An A_3 AR-selective ligand docked to an A_3 AR homology model.³⁷ (b) Alignment of A_1 - and A_3 AR homology models. Key residues for binding and selected nonconserved residues are depicted in white and cyan sticks for the A_3 - and A_1 AR, respectively. (c) Schematic representation of the A_3 - and A_1 AR binding sites. The black solid line outlines the binding site of the A_3 AR, and the A_1 AR is represented in cyan.

A_3 AR-selective ligands, i.e., the models with the lowest aLogAUC values were considered. The enrichment of A_3 AR-selective ligands was significantly worse for the A_1 AR model compared with the A_3 AR model, indicating that subtype selectivity was captured (Figure S2b). However, to ensure that a ligand of the target receptor will not bind to the antitarget, it is not sufficient to screen a single structure, as the compound may be recognized by a different binding site conformation. To take this into consideration, 10 different models representing different shapes of the orthosteric site were selected on the basis of the quality of the binding poses of known A_1 AR ligands and their lower enrichment of A_3 AR-selective ligands (Figures S2b and S3).

Analysis of the A_1 - and A_3 AR models revealed highly similar orthosteric sites, with close to 50% identical amino acid residues in the binding pocket. The predicted binding modes

for A_3 AR-selective ligands provided insights into structural elements that could be exploited to achieve subtype selectivity (Figure 2). One such nonconserved region was identified in the vicinity of Val169^{5,30} (the superscript denotes the Ballesteros–Weinstein numbering²⁸) in the A_3 AR model. The A_1 AR has Glu172^{5,30} in the same position and was predicted to form a salt bridge to His264^{6,66}, which is also conserved in the template A_{2A} AR crystal structure.²¹ This difference resulted in a more enclosed and polar environment at the top of the orthosteric site of the A_1 AR compared with the A_3 AR. For the A_3 AR, Val169^{5,30} and Ile253^{6,58} (Glu and Thr, respectively, in the A_1 AR) created a more hydrophobic environment in this region. The potential importance of these residues for selectivity was further supported by evidence that several docked A_3 AR-selective ligands occupied this subpocket with bulky groups. There were also more deeply buried nonconserved residues in the orthosteric site, e.g., Ser247^{6,52} of the A_3 AR. As the A_1 AR had His251^{6,52} in the corresponding position, this created an additional subpocket in the A_3 AR model that was occluded in the antitarget (Figure 2).

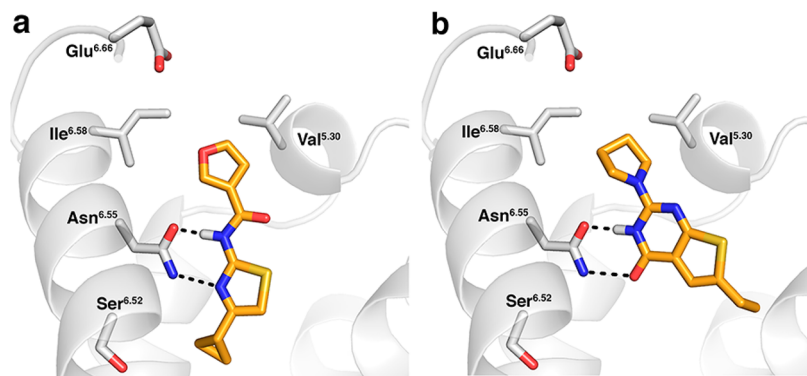
Docking Screen for A_3 AR-Selective Fragments. After deriving homology models of both the A_1 - and A_3 AR subtypes, we turned to prospective screening for novel A_3 AR fragment ligands. We were particularly interested in investigating whether a structure-based approach enables prediction of selective scaffolds, as ligands with specificity for the targets are typically not expected to emerge from fragment screening campaigns.⁹ More than 0.5 million commercially available fragments from the ZINC database²⁹ were screened against the A_3 AR structure and the ensemble of 10 A_1 AR models using DOCK3.6.²⁶ Each compound in the library was docked in thousands of orientations, resulting in a total of five billion predicted receptor–fragment complexes. A fragment was considered to be selective for the A_3 AR if it was top-ranked for the model of this receptor and the difference in docking rank was >10 000 positions worse for all of the screened A_1 AR models. On the basis of this criterion, only 27 of the 500 top-ranked compounds for the A_3 AR were selective, which likely reflected the high degree of similarity between the binding sites of these AR subtypes. In addition, as only fragments were considered, there were few compounds that could form the key interactions required for ligand binding and extend into nonconserved regions. The 4000 top-ranked compounds from the A_3 AR screen (0.8% of the screened database) had to be considered to identify 500 fragments that fulfilled the selectivity criterion. A large fraction of the 500 molecules interacted with Asn250^{6,55} and typically extended into at least one nonconserved region of the orthosteric site. Predicted binding poses were also inspected for the 10 A_1 AR models to ensure that the same receptor–ligand interactions could not be achieved for the antitarget. After visual inspection, a diverse set of 21 compounds (compounds 1–21; Table S1) were selected for experimental evaluation on the basis of their shape complementarity to the A_3 AR binding site, taking into account neglected terms in the docking scoring function as described previously.^{14,22,30} These compounds were also screened for substructures present in the set of previously characterized pan-assay interference compounds (PAINS)³¹ and did not contain any of these motifs. The average ranks for the selected compounds were 2293 for the A_3 AR and 29 579 for the A_1 AR, with a median rank difference of 24 319.

The predicted ligands were evaluated using a live-cell fluorescence-based competition assay at the A_3 - and A_1 AR.

Table 1. Binding Affinities for the Four Most Potent Fragments from the Docking Screen; K_i Values Were Obtained from the Fluorescence-Based Competition Binding Assay in Cells Expressing the A_3AR or A_1AR

ID	Docking rank ^a		Ligand structure	A_3AR^b	A_1AR^b	A_3/A_1 Fold selectivity ^c
	A_3AR	A_1AR		pK_i (n)	pK_i (n)	
1	1,102	44,106		6.98 ± 0.08 (6)	5.53 ± 0.10 (6)	29
2	808	29,751		5.64 ± 0.17^d (3)	>4 (3)	>38
3	2,609	19,192		5.62 ± 0.12 (3)	5.50 ± 0.06 (3)	1.2
4	2,062	16,784		5.66 ± 0.17 (3)	4.53 ± 0.30 (3)	24

^aRank of the compound in the docking screen of >0.5 million fragments from the ZINC database. ^bValues represent mean \pm standard error of the mean (SEM) from n separate experiments performed in duplicate. ^cFold selectivity represents the K_i value at the A_1AR divided by the K_i value at the A_3AR . ^dCompound 2 could not be tested at concentrations higher than 100 μM because of solubility issues. The pK_i value was derived by assuming that higher concentrations would displace binding to nonspecific levels.

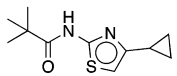
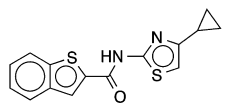
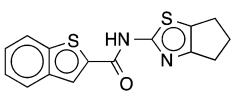
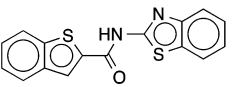
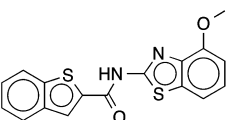
**Figure 3.** Predicted receptor–ligand complexes for two discovered ligands. The binding modes predicted by molecular docking for compounds (a) 1 and (b) 2 in the A_3AR model are shown. The A_3AR backbone is depicted as a white cartoon, and carbon atoms of key residues are shown as white sticks. The atoms of the ligand are shown as sticks with carbon atoms in orange.

This assay uses an image-based approach to measure the ability of each compound to compete with the binding of a xanthine amine congener-based fluorescent ligand, CA200645.⁵ Known A_3AR -selective (MRS1220) or A_1AR -selective (DPCPX) antagonists were tested on both A_3AR - and A_1AR -expressing cells to confirm that each cell line had the expected pharmacology for the given receptor (Figure S4). Compounds were initially evaluated at a single concentration (typically 1 mM), and the nine compounds that displaced the binding of CA200645 at the A_3AR to within 15% of that achieved by the reference A_3AR -selective compound MRS1220 (1 μM) were taken forward for further evaluation (Table S1 and Figure S5). Full concentration–response curves were generated for compounds 1–9 (Figure S6). The K_i values for compounds 1–4 ranged from 0.12 to 1.3 μM at the A_3AR . Compounds 5–8 were less potent A_3AR ligands, and their K_i values could not be precisely determined. Compound 9 was found to interfere

with the assay and was therefore excluded from further consideration. The eight identified A_3AR ligands corresponded to a hit rate of 38%, and notably, six of them displayed the desired selectivity. No compounds with significant activity displayed higher affinity for the A_1 subtype over the A_3 subtype (Tables 1 and S1). The four most potent compounds (1–4) were further examined, and their predicted binding modes are shown in Figures 3 and S7. Whereas compound 3 displayed similar affinities for the two subtypes, compounds 1, 2, and 4 were remarkably selective for the A_3AR with K_i ratios ranging from 24 to >38. In addition, the ligand efficiencies for the four most potent fragments (calculated as $LE = -(RT \ln K_i)/N$, where N is the number of ligand heavy atoms) varied between 0.47 and 0.62 kcal mol⁻¹ atom⁻¹, which indicated that they were promising starting points for optimization.³²

The chemical novelty of compounds 1–4 was assessed on the basis of their two-dimensional similarities to all A_1 -, A_2A -,

Table 2. Binding Affinities for Analogues of Compound 1; K_i Values Were Obtained from the Fluorescence-Based Competition Binding Assay in Cells Expressing the A_3AR or A_1AR

ID	Ligand structure	A_3AR^a		A_1AR^a		A_3/A_1 Fold selectivity ^b
		pK_i	n	pK_i	n	
22		5.31 ± 0.16	5	4.91 ± 0.12	4	2
23		7.47 ± 0.13	4	5.43 ± 0.10	4	101
24		6.42 ± 0.24	5	5.55 ± 0.13	4	5
25		6.48 ± 0.19	4	5.21 ± 0.10	4	16
26		6.96 ± 0.08	8	5.51 ± 0.21	7	34

^aValues represent mean \pm SEM from n separate experiments performed in duplicate. ^bFold selectivity represents the K_i value at the A_1AR divided by the K_i value at the A_3AR .

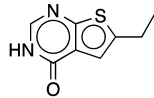
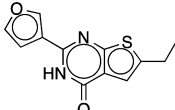
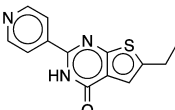
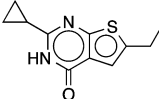
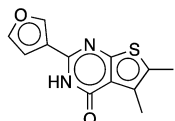
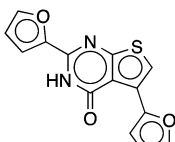
A_{2B} , and A_3AR ligands in the ChEMBL20 database. Similarity was quantified using the Tanimoto coefficient (T_c) calculated with extended connectivity fingerprints, maximum distance 4 (ECFP4). The maximal T_c value of 1 is obtained if there is an identical known ligand, whereas small values indicate low similarity to previously characterized compounds. The calculated T_c values for the identified ligands ranged from 0.28 to 0.4 (Table S2). Compounds 2–4 were judged to be dissimilar to the most similar AR ligands, and these molecules also had T_c values of <0.4 , which is typical for novel chemotypes.³³ Compounds 1 and 4 belong to a previously characterized thiazole scaffold, but it should be noted that both A_1 - and A_3AR -selective compounds bearing this group have been discovered.^{34,35} In fact, none of the discovered selective fragments would have been expected to be A_3AR -specific on the basis of the K_i value of the closest ligand (Table S2). The known AR ligand closest to compound 1 ($T_c = 0.40$) was selective for the A_1AR (rat, $0.039 \mu M$) over the A_3AR (human, 42% at $1 \mu M$).³⁶ Furthermore, the ChEMBL ligand most similar to compound 2 was a very close analogue of our reference ligand, the highly selective A_1AR antagonist DPCPX (Figure S4). Finally, it should be noted that the use of ligand-guided homology modeling did not appear to bias the docking screen, as none of the discovered compounds belonged to the class of A_3AR -specific pyrazolotriazolopyrimidines³⁷ that constituted the main selective scaffold used to guide model selection (Figure 2a).

Fragment-to-Lead Optimization. Although the successful identification of fragment ligands for the A_3AR was encouraging, a requisite for successful FBLD is the optimization of these in terms of selectivity and potency.¹ Fragment-to-lead optimization was guided by the receptor models and focused on the structure–activity relationship (SAR) for the two most potent and selective fragments, 1 and 2. Five analogues of

compound 1 and six of compound 2 were tested at the A_3 - and A_1AR in the fluorescence-based competition binding assay (Tables 2 and 3).

Compound 1 had a K_i value of 120 nM ($LE = 0.62 \text{ kcal mol}^{-1} \text{ atom}^{-1}$) and was predicted to target two nonconserved regions in the A_3AR binding pocket. The cyclopropyl group occupied the pocket created by Ser247^{6,52} in the A_3AR model (His251^{6,52} for the A_1AR), whereas the furan ring was positioned in the hydrophobic cleft formed by Val169^{5,30}, Ile253^{6,58}, and Leu264^{7,35} (Figure 3a). These two groups were connected via a 1,3-thiazole-2-carboxamide moiety, which formed hydrogen bonds to Asn250^{6,55} and π -stacking interactions with Phe168^{5,29}. Despite the fact that this ligand has only 16 heavy atoms, 29-fold selectivity was observed experimentally. Compound 22 was first evaluated to assess the role of the furan group, which extended into the nonconserved hydrophobic pocket in the top of the orthosteric site. The predicted binding mode of compound 22 suggested that the slightly smaller substituent would not access the nonconserved pocket to the same extent as compound 1 (Figure 4a). The significant loss of A_3AR affinity and specificity for compound 22 supported the importance of the furan group (Table 2). To further optimize the ligand from a fragment to a lead-like compound, commercially available analogues with larger substituents were docked to the A_3AR model. Compound 23, with a benzothiophene group replacing the furan, extended further into the hydrophobic pocket at the top of the A_3AR orthosteric site (Figure 4b). In agreement with this observation, this ligand was 3-fold more potent at the A_3AR , which resulted in an overall 100-fold selectivity for this subtype (Table 2 and Figure 5a). Focus was then put on optimizing interactions in the nonconserved regions in the bottom of the A_3AR binding site, which was predicted to accommodate the cyclopropyl group. In compounds 24 and 25, the cyclopropyl-substituted

Table 3. Binding Affinities for Analogues of Compound 2; K_i Values Were Obtained from the Fluorescence-Based Competition Binding Assay in Cells Expressing the A_3AR or A_1AR

ID	Ligand structure	A_3AR^a		A_1AR^a		A_3/A_1 Fold selectivity ^b
		pK_i	n	pK_i	n	
27		4.87 ± 0.09	4	4.12 ± 0.11	4	6
28		6.26 ± 0.09	4	4.25 ± 0.08	4	102
29		5.70 ± 0.10	4	4.64 ± 0.20	4	14
30		5.74 ± 0.24	5	4.21 ± 0.10	4	70
31		6.40 ± 0.11	4	5.71 ± 0.04	4	4
32		6.86 ± 0.06	4	6.46 ± 0.08	4	2

^aValues represent mean \pm SEM from n separate experiments performed in duplicate. ^bFold selectivity represents the K_i value at the A_1AR divided by the K_i value at the A_3AR .

thiazole is replaced by 5,6-dihydro-4*H*-cyclopentathiazole and benzothiazole groups, respectively. Interestingly, these ligands displayed >10-fold lower affinity for the A_3AR compared with the parent compound, leading to a loss of selectivity (Table 2). Analysis of the docking poses suggested that the bicyclic substituents did not penetrate as deep as the cyclopropyl group into the nonconserved pocket below Asn250^{6,55} of the A_3AR (Figures 4 and S8). Instead of reverting to the more potent cyclopropyl group, we evaluated compound 26, which was predicted to position a methoxy group in the same pocket. This analogue restored the affinity ($K_i = 120$ nM) and improved the selectivity (34-fold) toward the A_3AR (Figure 4c and Table 2). Overall, 3-fold improvements of potency and selectivity were achieved in the optimization, and the most promising lead was compound 23, which had a K_i value of 40 nM and >100-fold selectivity for the A_3AR over the A_1AR (Figure 4d).

Compound 2 was the most promising fragment in terms of selectivity and also had a high LE ($0.47 \text{ kcal mol}^{-1} \text{ atom}^{-1}$). On the basis of its predicted binding mode, the selectivity appeared to originate from the pyrrolidine ring in the nonconserved pocket at the opening of the A_3AR binding site (Figure 3b). To investigate the contribution of this substituent to the selectivity,

an analogue that lacked this group (compound 27) was evaluated. As anticipated, this fragment lost a majority of its selectivity (Table 3). Our models thus suggested that both compounds 1 and 2 achieved their selectivity by interacting with residues in the same nonconserved subpocket (Figure 2). This led us to hypothesize that the SAR for analogues of compound 1 may be transferable to this scaffold. On the basis of this observation, the pyrrolidine was replaced by a furan group in compound 28, which docked well into the A_3AR model (Figure S9a). Compound 28 displayed 5-fold-improved potency at the A_3AR and remained strongly selective for this subtype (Table 3 and Figure 5b). Compounds 29 and 30 were then tested to further investigate the SAR for substituents at the same position. Increasing the size of the substituent to a pyridine in compound 29 led to a 4-fold loss of A_3AR affinity compared with compound 28, which decreased the selectivity, while reducing the size to a nonplanar cyclopropyl moiety in compound 30 retained significant specificity toward the A_3AR (70-fold) (Table 3). Focus was then put on further exploring the SAR for the most promising fragment, compound 28, by evaluating analogues that retained the furan moiety. Compound 31 maintained its affinity at the A_3AR but was also 30-fold more

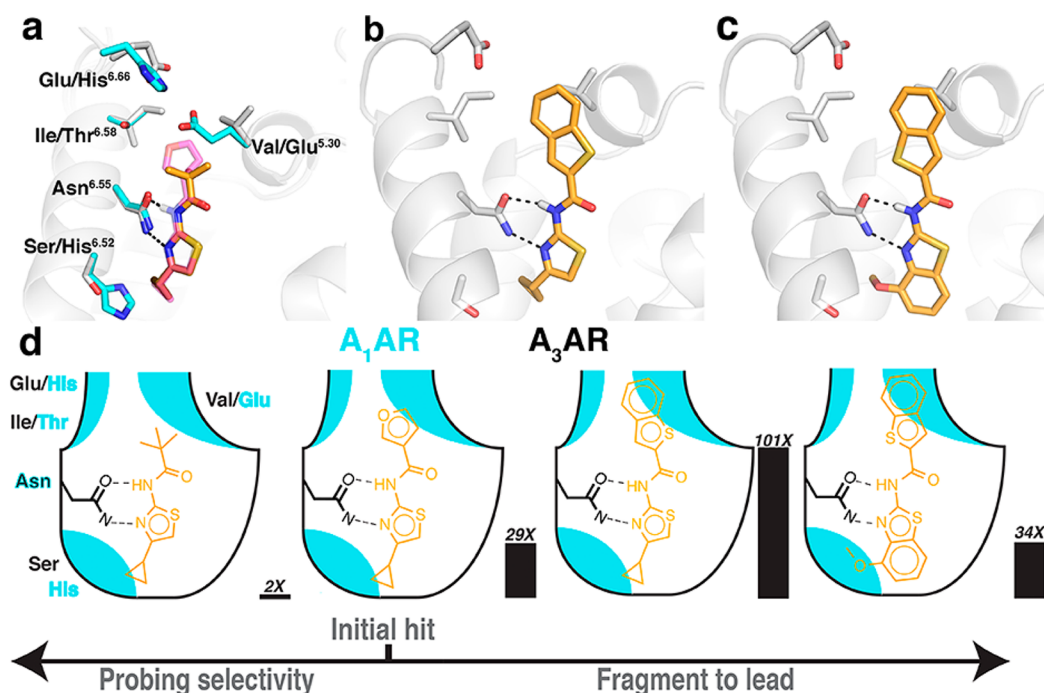


Figure 4. Fragment-to-lead optimization. (a–c) Predicted binding modes for analogues of the most potent fragment (compound 1) from the initial screen: (a) compound 22 and compound 1 (transparent magenta carbon atoms); (b) compound 23; (c) compound 26. The backbone atoms of the A_3AR are shown as a white cartoon, whereas carbon atoms of key residues are shown as white sticks. Unless noted otherwise, the ligand atoms are shown as sticks with carbon atoms in orange, and A_1AR residues are shown as sticks with cyan carbon atoms. (d) Schematic representation of structure-guided fragment-to-lead optimization based on the homology models of the A_3AR (black line outlining the binding site) and A_1AR (transparent cyan highlighting relevant differences between the target and antitarget). From left to right: compounds 22, 1, 23, and 26.

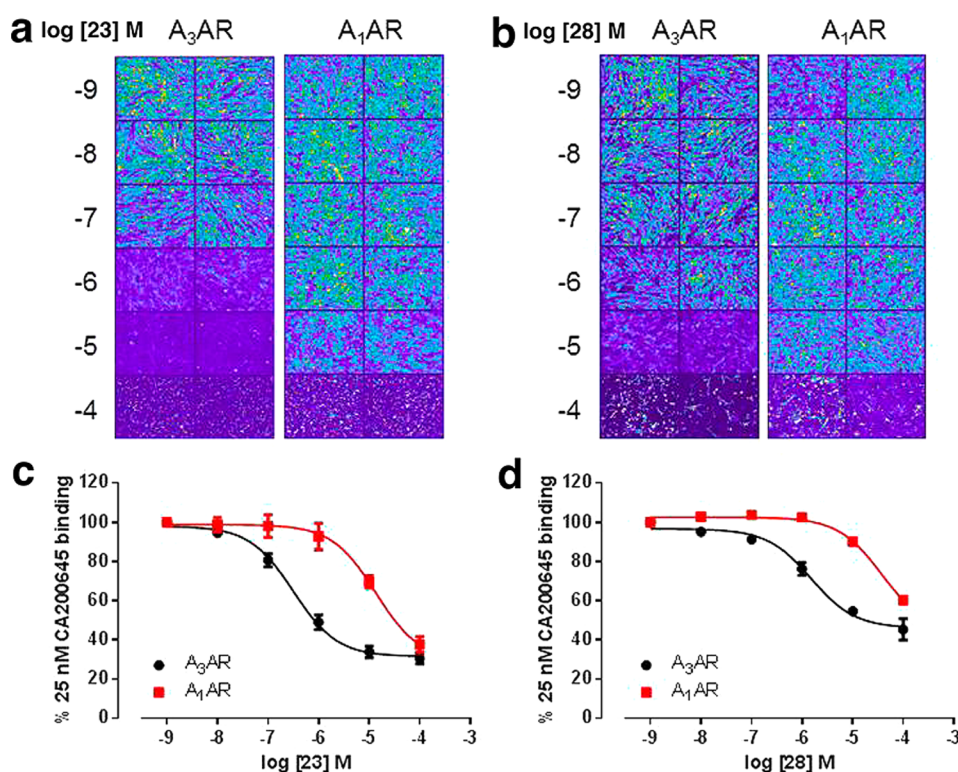


Figure 5. Concentration response curves for the most selective ligands. (a, b) High content screening images from A_3AR and A_1AR cells treated with increasing concentrations of (a) 23 or (b) 28 in the presence of 25 nM CA200645. Images represent CA200645 fluorescence and are representative of those obtained in four separate experiments. (c, d) Competition binding curves generated from the resulting levels of fluorescence from cells expressing the A_3AR (black circles) or A_1AR (red squares) upon treatment with increasing concentrations of (c) 23 or (d) 28 in the presence 25 nM CA200645. Each data point represents the mean \pm SEM from four separate experiments performed in duplicate.

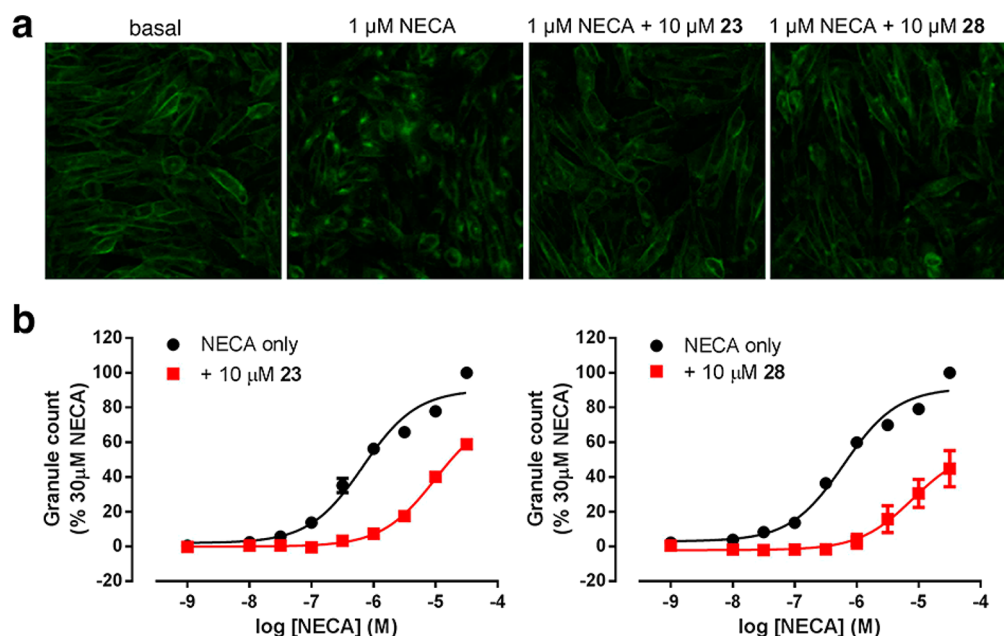


Figure 6. Functional antagonism of the A₃AR by compounds 23 and 28. (a) Representative images of CHO cells expressing A₃-YFP were treated with 10 μM 23 or 28 and 1 μM NECA. Clear internalization of A₃-YFP upon NECA treatment can be seen, and this is blocked in the presence of 23 or 28. (b) Concentration response curves from A₃-YFP-expressing cells treated with increasing concentrations of NECA in the presence (red squares) or absence (black circles) of 10 μM 23 or 28. Granule count was estimated from the resulting images obtained on the ImageXpress confocal plate reader. Each data point represents the mean ± SEM of five experiments performed in triplicate.

potent at the A₁AR, which significantly reduced the selectivity (Table 3). Similarly, compound 32, which was evaluated in order to extend further toward the second nonconserved pocket around Ser247^{6,52}, was almost equally potent at both subtypes (Table 3). These results supported the conclusion that in addition to the furan group, the ethyl substituent of compound 28 was also important for A₃AR specificity. This further demonstrated that effects on the selectivity due to substituents at one position can strongly depend on substituents at other positions of a fragment ligand, which is in line with observations made for analogues of compound 1. This could be due to the ability of certain substituents to anchor the core scaffold of a fragment in a particular orientation, resulting in selectivity when nonconserved binding site regions are targeted by other substituents. However, in the absence of such an anchoring group, selectivity gained by the other substituent could be reduced or ablated because the fragment can reorient in the binding site. Visual inspection of the docking poses for compounds 28 and 31 further supported this hypothesis. In contrast to the selective parent compound 28, compound 31 could be better accommodated in seven out of the 10 A₁AR models (and equally well in the remaining three), as judged by key interactions with Asn^{6,55}. Anchored by the ethyl substituent, the orientation of compound 28 appeared to be more restricted in the A₁AR binding site, whereas compound 31 was able to reorient in response to the subtle change in chemical structure (Figure S9). Overall, the best ligand emerged from optimization of interactions in the nonconserved cavity at the top of the binding site, and despite the fact that compound 28 was still fragment-sized, it had submicromolar affinity with >100-fold A₃AR selectivity.

To further probe the selectivity profiles of our discovered ligands, the two most promising leads, compounds 23 and 28, and the fragment ligands from which they were derived, compounds 1 and 2, were evaluated in radioligand binding

assays at the A_{2A}AR. Compounds 1, 2, and 28 did not show any significant displacement of the radioligand at 10 μM, whereas compound 23 was determined to have a K_i value of 2.9 μM, resulting in 72-fold selectivity for the A₃AR over the A_{2A} subtype. All four of these compounds were thus selective for the A₃AR over both the A₁ and A_{2A} subtypes.

Functional Assays for Compounds 23 and 28. As the A₃AR homology model was based on a crystal structure determined in an inactive state and a recent study demonstrated that commercial screening libraries are biased toward AR antagonists over agonists,³⁸ we expected the discovered ligands to behave as antagonists. This was confirmed by evaluating the functional behavior of our most promising leads, compounds 23 and 28, for their ability to antagonize 5'-N-ethylcarboxamidoadenosine (NECA)-mediated internalization of the A₃AR linked to yellow fluorescent protein (YFP). Both ligands caused a rightward shift in the agonist-mediated concentration response curve (Figure 6) with no increase in internalization at low NECA concentrations, indicating competitive antagonism. From these shifts, the affinities (pK_D) of the antagonists 23 and 28 were estimated to be 6.13 ± 0.01 and 6.13 ± 0.08 (mean ± SEM, n = 5), respectively.

DISCUSSION

Three key results emerge from our study. Fragment ligands were first successfully identified on the basis of molecular docking screens against a homology model of the A₃AR. Eight out of the 21 predicted ligands were verified to bind in a live-cell environment using fluorescent ligand assays, corresponding to a high hit rate of 38%, and several fragments had high affinities. The second and perhaps most important finding in this work is that an additional screen against homology models of an antitarget could be used to bias the screen toward the identification of subtype-selective fragments. Despite the low

molecular complexity of the screened fragments, six of the eight discovered ligands were selective for the A₃AR over the A₁AR, and several displayed remarkably large differences in potency. Finally, the homology models contributed to an understanding of the structural basis for the selectivity and were used to guide fragment-to-lead optimization.

It could be argued that prediction of fragment ligands should pose a significant challenge to molecular docking algorithms. As fragments only occupy a fraction of a binding site, they can be docked in a large number of orientations, and it may be difficult for the simplified scoring function to rank these by affinity. Despite these shortcomings of docking, the first virtual screens of fragment libraries against GPCR crystal structures have been successful, reaching hit rates as high as 73% for the H₁ histamine receptor.^{14,15} The high hit rates achieved in these studies partly reflect the druggability of the orthosteric sites of GPCRs and favorable library bias,³⁹ making these targets particularly suitable for fragment screening. In addition to the higher hit rates observed for fragments and the lower computational cost of the *in silico* screens, there are other advantages of focusing on such libraries. For example, as fragment libraries offer better coverage of chemical space, docking screens of these may lead to the discovery of chemotypes that are not present in lead-like libraries.¹³ The present study involved additional layers of complexity wherein fragment ligands were sought to a receptor of unknown structure and were required to be less potent at a closely related subtype also lacking a crystal structure. To put our results in perspective, Stoddart et al.⁵ carried out an empirical screen of 248 fragments against the A₃AR using the same fluorescent binding assay as in this work, which resulted in the discovery of 34 ligands with affinities between 0.4 and 107 μ M. The 14% hit rate from the screen was relatively high compared with other experimental fragment screens against GPCRs,^{2,3} and 17 of the ligands had K_i values of <10 μ M. The most potent fragment (K_i = 360 nM) was also tested for A₃AR selectivity and was found to display similar affinity for the A₁AR. The docking screen carried out here considered a 2000-fold larger library (>0.5 million compounds) but required the experimental evaluation of only 21 compounds. The eight discovered A₃AR ligands corresponded to a nearly 3-fold higher hit rate, and a larger fraction of the hits (four compounds) had K_i values of <10 μ M. Notably, the most potent fragment from the docking screen had a K_i value of 120 nM with 29-fold selectivity for the A₃AR. Overall, the most potent fragments identified by molecular docking and those from Stoddart et al. had similar novelty but did not significantly overlap in terms of chemotypes. This result further supports the conclusion that combining empirical screens of small libraries with *in silico* screening of all commercially available fragments can increase the number and diversity of starting points for optimization.^{14,40}

Accurate approaches for homology modeling will be required to fully capitalize on the recent advances in membrane protein crystallography and may prove to be essential for addressing key challenges in early-phase drug discovery.⁴¹ A particularly important role of homology models is in structure-based design of selective ligands, as representative crystal structures for all receptor subtypes are not available for any human GPCR family.¹¹ Prospective docking screens against homology models of GPCRs have to date yielded different levels of success^{16,22,30,42} and to our knowledge have not previously involved modeling of both a target and antitarget to drive structure-based discovery of selective fragments. If a crystal

structure of a receptor closely related to the target is available, it could be argued that homology models should be suitable for docking screens because subpockets that are conserved are likely to be well-described. In such cases, minor discrepancies in nonconserved regions of the binding site may not influence the docking hit rate. On the contrary, structure-based screens for selective ligands generally involve interactions in regions that are not conserved, which are difficult to model accurately on the basis of homology.^{42,43} This problem was recently highlighted by the work of Rodriguez et al.,⁴³ which demonstrated that homology models of the serotonin 5-HT_{1B} and 5-HT_{2B} receptors lacked the accuracy required to capture the subtle binding site differences responsible for subtype selectivity that were revealed by crystal structures of these GPCRs. In the light of these results, it was clear that tailored modeling strategies for both the target and antitarget receptors would be necessary to predict subtype-selective GPCR ligands. We used ligand-guided homology modeling to bias the A₃AR model toward a conformation with the ability to recognize selective scaffolds using an approach similar to that of Katritch et al.²³ A unique component of our strategy was a representation of the antitarget that captured binding site flexibility by using an ensemble of structures⁴⁴ optimized to discriminate between selective and non-A₃AR-selective ligands. Our docking screens against the resulting A₃- and A₁AR models led to the discovery of eight fragment ligands, of which six displayed the desired subtype selectivity. However, despite the use of 10 different antitarget models, two fragment hits were only marginally more potent at the A₃AR than at the A₁ subtype, suggesting that additional and more disparate conformations might need to be considered in order to further improve predictions of selectivity. Furthermore, we have not explicitly considered binding site water molecules, which could play important roles in determining ligand specificity.^{45–47} The use of ligand data to generate the homology models is also a limitation of our approach, but it should be noted that the amount of publicly available small-molecule binding data for GPCRs is increasing rapidly.⁴⁸ Our approach is highly automated, and we anticipate that it could be extended to a large number of GPCR families, including many targets for which drug discovery has been hampered by adverse effects caused by off-target interactions.

Efficient optimization of fragment hits is crucial for the successful use of FBLD in drug discovery.^{1,7} The discovery of several ligands in our screen provided the opportunity to test whether homology models could guide fragment-to-lead optimization. Whereas potency (or ligand efficiency) is typically used to prioritize hits from fragment screens,³² opinion is currently divided regarding whether selectivity should be considered. It has been argued that selectivity is too challenging to predict and that this property may be lost (or gained) in fragment-to-lead optimization.⁴⁹ As previously observed for kinases,⁴⁹ a complex SAR was observed in the optimization of selectivity, and small structural changes greatly affected the specificity, which may reflect the fact that fragments can reorient in the binding site during optimization to a larger extent than leads.⁵⁰ This likely makes rational optimization more challenging for fragment ligands than for lead- or drug-like molecules. Encouragingly, we found that the associated differences in selectivity could be explained by the homology models in several cases and guide further optimization. Our results suggest that selectivity can be a valuable property of hits from fragment screens provided that the structural basis of

ligand binding is understood and systematically utilized to guide optimization. For two selective fragments identified in our screen, the chemical groups responsible for the subtype selectivity were first predicted on the basis of modeled receptor–fragment complexes and subsequently confirmed experimentally by evaluating analogues lacking those moieties. Compounds that further exploited nonconserved pockets were then identified using docking to the A₃AR models, which led to the discovery of potent lead compounds with >100-fold selectivity and up to 40 nM affinity for the A₃AR. Interestingly, the two optimized leads, compounds **23** and **28**, and the fragments from which they were derived were also selective for the A₃AR over the A_{2A}AR, which may reflect binding site similarities between the A₁ and A_{2A} subtypes.

CONCLUSIONS

The main finding of this work is that docking screens against homology models of GPCRs can be utilized to discover subtype-selective fragments. The structural understanding of ligand selectivity gained from the homology models can also be used to guide fragment-to-lead optimization. The described strategy for *in silico* FBLD for GPCRs of unknown structure can be readily extended to a large number of pharmaceutically important targets.

METHODS

Sequence Alignment and Homology Modeling. The sequences of the human A₃- and A₁AR were aligned to that of the template crystal structure, the human A_{2A}AR, using PROMALS3D.⁵¹ The sequence alignment was manually edited in loop regions. The C- and N-terminals and the third intracellular loop were excluded from the modeling because they were missing in the template structure. Homology modeling of the human A₃AR and A₁AR was performed on the basis of a 1.8 Å resolution structure of the A_{2A}AR (PDB accession code 4EYI²¹) using MODELER version 9.11.⁵² A total of 1000 models were generated for each receptor. Additional dihedral restraints were placed on the conserved Asn⁶⁵⁵ to keep the rotamer of this residue close to that observed in a majority of the available A_{2A}AR crystal structures. For the A₃AR, restraints were placed on the side-chain rotamer of nonconserved Ser247⁶⁵² to keep it similar to the template and the distance between residues Arg173⁵³⁴ and Asp175⁵³⁶ to prevent these residues from blocking the orthosteric site. For the A₁AR, additional dihedral and distance restraints were placed on Glu172⁵³⁰ and His264⁶⁶⁶ to maintain the salt bridge observed in the template crystal structure of the A_{2A}AR and on Lys265⁶⁶⁷ to prevent it from blocking the orthosteric site.

Ligand-Guided Homology Modeling and Molecular Docking Screening. All of the docking calculations were carried out with the program DOCK3.6.²⁶ Unless stated otherwise, the protonation states of the ionizable residues Asp, Glu, Arg, and Lys in the binding site were set to their most probable states in the receptor at pH 7. Histidine tautomeric states in the binding site were set on the basis of the hydrogen-bonding network. His251⁶⁵², His264⁶⁶⁶, and His278⁷⁴³ in the A₁AR were protonated at N ϵ , both side-chain nitrogens, and N δ , respectively. Of these, only His272⁷⁴³ was also present in the A₃AR and was protonated in the N δ position. The flexible ligand sampling algorithm in DOCK3.6²⁶ superimposes atoms of the docked molecule onto binding site matching spheres, which indicate putative ligand atom positions. A total of 45 matching spheres were used and were based on the atoms of the cocrystallized antagonist ZM241385. The spheres were also labeled for chemical matching based on the local receptor environment.⁵³ The degree of ligand sampling was determined by the bin size, bin size overlap, and distance tolerance. These three parameters were set to 0.4 Å, 0.2 or 0.3 Å, and 1.5 Å, respectively, for both the binding site matching spheres and the docked molecules. An initial filter discarded conformations that had more than one overlapping heavy atom with the receptor. An overlap

between two atoms was defined as a distance shorter than 2.3 or 2.6 Å for polar or nonpolar atoms, respectively, and was determined from a precalculated grid. For ligand conformations passing this steric filter, a physics-based scoring function was used to evaluate the fit to the binding site. For the best-scoring conformation of each docked molecule, 100 steps of rigid-body minimization were carried out. The score for each conformation was calculated as the sum of the receptor–ligand electrostatic and van der Waals interaction energies, corrected for ligand desolvation. These three terms were evaluated from precalculated grids. The three-dimensional map of the electrostatic potential in the binding site was prepared using the program Delphi.⁵⁴ In this calculation, partial charges from the united-atom AMBER force field⁵⁵ were used for all receptor atoms except the side-chain amides of Asn250⁶⁵⁵ and Asn254⁶⁵⁵ for the A₃AR and A₁AR, respectively, for which the dipole moment was increased to favor hydrogen bonding to this residue, as described previously for the A_{2A}AR.^{14,39} The program CHEMGRID was used to generate a van der Waals grid based on a united-atom version of the AMBER force field.⁵⁵ The desolvation penalty for a ligand conformation was estimated from a precalculated free energy for transfer of the molecule between solvents with dielectric constants of 78 and 2. The desolvation energy was obtained by weighting the transfer free energy with a scaling factor that reflects the degree of burial of the ligand in the receptor binding site.²⁷

Sets of lead-like ligands (molecular weight <350) for the A₃AR and A₁AR were extracted from the ChEMBL14 database⁴⁸ and consisted of 520 and 622 compounds, respectively. The set of 138 subtype-selective ligands of the A₃AR (molecular weight <500, >50-fold selective for the A₃AR over the A₁ subtype) was extracted from ChEMBL14.⁴⁸ Decoys were generated in a 1:50 ratio for each of the three ligand sets using the DUD-E approach.²⁵ In the prospective screens, the ZINC fragment library⁵⁹ of 504 973 commercially available compounds (molecular weight \leq 250, LogP \leq 3.5, and \leq 5 rotatable bonds) was used. All of the docked compounds were prepared for docking using the ZINC database protocol.²⁹

Similarity Calculations. Similarity calculations for the fragments were carried out using the Screenmd program from Chemaxon.⁵⁶ We calculated the maximum Tanimoto coefficient with ECFP4 fingerprints between each discovered fragment ligand and all compounds that have been annotated against any AR subtype in the ChEMBL20 database.⁴⁸

Materials. The fragment hits from the initial screen and the analogues of compounds **1** and **2** were purchased from Enamine, Life Chemicals, VitasM, Peakdale, Chembridge, and UK organic synthesis (Table S3). Compound identities and purities were confirmed by NMR and liquid chromatography–mass spectrometry (LC–MS) for all discovered ligands (Table S3). FCS was purchased from PAA Laboratories (Wokingham, UK) and L-glutamine from Lonza (Basel, Switzerland). MRS1220, DPCPX, and NECA were obtained from Tocris Bioscience (Bristol, UK). CA200645 was purchased from Cellaura Technologies Ltd. (Nottingham, UK). All other chemicals and reagents were purchased from Sigma-Aldrich (Gillingham, UK).

Cell Lines and Cell Culture. Chinese hamster ovary (CHO) cells expressing the A₁AR⁵⁷ and CHO CRE-SPAP cells expressing the A_{2A}AR⁵⁸ or A₃-YFP⁵⁹ were prepared as previously described. All of the cell lines were maintained in Dulbecco's modified Eagle's medium (DMEM) nutrient mix F12 (DMEM-F12) supplemented with 10% fetal calf serum and 2 mM L-glutamine at 37 °C in a humidified atmosphere of air/CO₂.

Fluorescence-Based Competition Binding Assay. Cells expressing the A₁AR or A₃AR were grown to confluency in the central 60 wells of a 96-well plate in normal growth medium. Because of issues with the quality of the images obtained from the outside wells of a 96-well plate, the outer wells were left blank. On the day of analysis, the medium was removed and the cells were washed twice with HEPES-buffered saline solution (HBSS; 25 mM HEPES, 10 mM glucose, 146 mM NaCl, 5 mM KCl, 1 mM MgSO₄, 2 mM sodium pyruvate, 1.3 mM CaCl₂, 1 mM NaHCO₃, pH 7.4). For initial evaluation of compounds **1–21**, a single concentration of test compound (dependent on the solubility of the individual compound;

see Figure S5 and Table S1), 1 μ M MRS1220, 1 μ M DPCPX, or buffer was added in duplicate to the required wells, followed by 25 nM CA200645. For analysis of the affinities of compounds, increasing concentrations of the required compounds were added, followed by 25 nM CA200645. Cells were then incubated for 1 h at 37 °C (no CO₂) and then washed once in HBSS prior to imaging on an ImageXpress Ultra confocal plate reader (Molecular Devices, Sunnyvale, CA, USA). Four images were taken per well using a Plan Fluo 40× NA0.6 extra-long working distance objective by excitation of the fluorophore (BODIPY630/650) at 636 nm, and the emission was collected through a 640–685 nm band-pass filter. To obtain the total image intensity a modified multiwavelength cell scoring algorithm within MetaXpress software (Molecular Devices) was used.

Receptor Internalization Assay. CHO cells expressing A₃-YFP were grown to confluency in the central 60 wells of black-walled, clear bottom 96-well plates. On the day of the experiment, normal growth medium was replaced with serum-free medium (DMEM-F12 containing 2 mM L-glutamine) containing, where required, a fixed concentration of 23 or 28, and the cells were incubated for 30 min at 37 °C/5% CO₂/95% air. This was followed by the addition of increasing concentrations of NECA, and the cells were incubated for a further 60 min. All of the medium was then removed, and the cells were washed once in phosphate-buffered saline (PBS) prior to fixation with 3% paraformaldehyde solution in PBS (20 min, room temperature). The cells were then washed twice in PBS, and the nuclei were stained by the addition of H33342 (2 μ g/mL⁻¹, 20 min, room temperature). The cells were washed a further two times and then imaged on the ImageXpress Ultra confocal plate reader. Four central images were taken per well using a Plan Fluor 40× NA0.6 extra-long working distance objective. YFP images were obtained by excitation at 488 nm, and the emission was collected through a 525–550 nm band-pass filter. H33342 was imaged by excitation at 405 nm and emission collection through a 447–460 nm band-pass filter. Analysis of the images was carried out using a granularity algorithm within MetaXpress software (Molecular Devices) to identify the granule count per cell on a per-image basis. A₃-YFP granules were classified as having a diameter of between 7 and 15 μ m and cell nuclei between 6 and 9 μ m, with the intensity above background set for each individual experiment.

Data Analysis. All of the concentration–response data were fitted using nonlinear regression models with Prism 6 (GraphPad Software, San Diego, CA, USA). Competition binding curves were fitted to the following equation to obtain the binding affinity (K_i) of the unlabeled ligand to the receptor:

$$K_i = \frac{IC_{50}}{1 + \frac{[L]}{K_D}}$$

where [L] is the concentration of CA200645 used (25 nM) and K_D is the affinity (in nM) of CA200645 at the A₁AR or A₃AR. The calculated K_D values used were 17.0 nM at the A₁AR and 3.11 nM at the A₃AR. The IC₅₀ was calculated using the following equation:

$$\% \text{ inhibition of specific binding} = \frac{100 \times [A]}{[A] + IC_{50}}$$

where [A] is the concentration of the competing drug and the IC₅₀ is the molar concentration of ligand required to inhibit 50% of the specific binding of 25 nM CA200645. Concentration–response internalization data were initially fitted to the following equation:

$$\text{response} = \frac{E_{\max} \times [A]}{[A] + EC_{50}}$$

where E_{\max} is the maximal response in the absence of competing ligand and the EC₅₀ is the molar concentration of agonist required to generate 50% of the E_{\max} . This was followed by estimation of the affinity (K_D) of the competing ligand using the Gaddum equation:

$$DR = 1 + \frac{[B]}{K_D}$$

where the dose ratio (DR) is the ratio of the agonist (NECA) concentrations required to stimulate an identical response in the presence and absence of the antagonist, B.

Radioligand Binding Assays for the A_{2A}AR. The affinities of the four compounds 1, 2, 23, and 28 were obtained at the human A_{2A}AR in vitro using radioligand binding assays according to experimental protocols described elsewhere.⁶⁰ Human A_{2A}AR expressed in transfected HeLa cells was employed, and [³H]-ZM241385 was used as the radioligand. Binding was evaluated as a percentage of the inhibition value at a single-point concentration of 10 μ M or the K_i value for compounds displaying >50% displacement of the radioligand at this concentration.

■ ASSOCIATED CONTENT

Supporting Information

The Supporting Information is available free of charge on the ACS Publications website at DOI: 10.1021/acs.jmedchem.5b01120.

Figures S1–S9 and Tables S1–S3 (PDF)

SMILES strings, p*K*_i values, and selectivity ratios for compounds 1–4 and 22–32 (CSV)

■ AUTHOR INFORMATION

Corresponding Authors

*E-mail: jens.carlsson@orgfarm.uu.se.

*E-mail: Steve.Hill@nottingham.ac.uk.

Author Contributions

||A.R. and L.A.S. contributed equally to this work.

Notes

The authors declare no competing financial interest.

■ ACKNOWLEDGMENTS

This work was supported by grants to J.C. from the Knut and Alice Wallenberg Foundation, the Swedish Foundation for Strategic Research, and the Swedish Research Council. L.A.S. and S.J.H. were supported by the Medical Research Council (Grant G080006). We thank the Chemical Biology Consortium Sweden for assistance with the LC–MS experiments and Jackie Glenn for technical assistance with the fluorescence-based experiments. Computational resources were provided by the Swedish National Infrastructure for Computing (SNIC) and the National Supercomputer Centre (NSC) in Linköping. We thank OpenEye Scientific Software for the use of Omega and OEchem at no cost. J.C., S.J.H., L.A.S., and A.R. participate in the European COST Action CM1207 (GLISTEN).

■ ABBREVIATIONS USED

FBLD, fragment-based lead discovery; GPCR, G protein-coupled receptor; AR, adenosine receptor; NMR, nuclear magnetic resonance; SPR, surface plasmon resonance; ROC, receiver operator characteristic; aLogAUC, adjusted logarithm of area under the curve; SAR, structure–activity relationship; PAINS, pan-assay interference compounds; T_c , Tanimoto coefficient; ECFP4, extended chemical fingerprints up to 4 atoms; CHO, Chinese hamster ovary; YFP, yellow fluorescent protein; DR, dose ratio; LC–MS, liquid chromatography–mass spectrometry; NECA, 5'-N-ethylcarboxamidoadenosine

■ REFERENCES

(1) Congreve, M.; Chessari, G.; Tisi, D.; Woodhead, A. J. Recent developments in fragment-based drug discovery. *J. Med. Chem.* **2008**, *51*, 3661–3680.

- (2) Congreve, M.; Rich, R. L.; Myszka, D. G.; Figaroa, F.; Siegal, G.; Marshall, F. H. Fragment screening of stabilized G-protein-coupled receptors using biophysical methods. *Methods Enzymol.* **2011**, *493*, 115–136.
- (3) Chen, D.; Errey, J. C.; Heitman, L. H.; Marshall, F. H.; Ijzerman, A. P.; Siegal, G. Fragment screening of GPCRs using biophysical methods: identification of ligands of the adenosine A(2A) receptor with novel biological activity. *ACS Chem. Biol.* **2012**, *7*, 2064–2073.
- (4) Aristotelous, T.; Ahn, S.; Shukla, A. K.; Gawron, S.; Sassano, M. F.; Kahsai, A. W.; Wingler, L. M.; Zhu, X.; Tripathi-Shukla, P.; Huang, X. P.; Riley, J.; Besnard, J.; Read, K. D.; Roth, B. L.; Gilbert, I. H.; Hopkins, A. L.; Lefkowitz, R. J.; Navratilova, I. Discovery of beta2 Adrenergic Receptor Ligands Using Biosensor Fragment Screening of Tagged Wild-Type Receptor. *ACS Med. Chem. Lett.* **2013**, *4*, 1005–1010.
- (5) Stoddart, L. A.; Vernall, A. J.; Denman, J. L.; Briddon, S. J.; Kellam, B.; Hill, S. J. Fragment screening at adenosine-A(3) receptors in living cells using a fluorescence-based binding assay. *Chem. Biol.* **2012**, *19*, 1105–1115.
- (6) Overington, J. P.; Al-Lazikani, B.; Hopkins, A. L. How many drug targets are there? *Nat. Rev. Drug Discovery* **2006**, *5*, 993–996.
- (7) de Kloe, G. E.; Bailey, D.; Leurs, R.; de Esch, I. J. P. Transforming fragments into candidates: small becomes big in medicinal chemistry. *Drug Discovery Today* **2009**, *14*, 630–646.
- (8) Hann, M. M.; Leach, A. R.; Harper, G. Molecular complexity and its impact on the probability of finding leads for drug discovery. *J. Chem. Inf. Model.* **2001**, *41*, 856–864.
- (9) Chen, Y.; Shoichet, B. K. Molecular docking and ligand specificity in fragment-based inhibitor discovery. *Nat. Chem. Biol.* **2009**, *5*, 358–364.
- (10) Murray, C. W.; Blundell, T. L. Structural biology in fragment-based drug design. *Curr. Opin. Struct. Biol.* **2010**, *20*, 497–507.
- (11) Katritch, V.; Cherezov, V.; Stevens, R. C. Structure-function of the G protein-coupled receptor superfamily. *Annu. Rev. Pharmacol. Toxicol.* **2013**, *53*, 531–556.
- (12) Dore, A. S.; Robertson, N.; Errey, J. C.; Ng, I.; Hollenstein, K.; Tehan, B.; Hurrell, E.; Bennett, K.; Congreve, M.; Magnani, F.; Tate, C. G.; Weir, M.; Marshall, F. H. Structure of the adenosine A(2A) receptor in complex with ZM241385 and the xanthines XAC and caffeine. *Structure* **2011**, *19*, 1283–1293.
- (13) Teotico, D. G.; Babaoglu, K.; Rocklin, G. J.; Ferreira, R. S.; Giannetti, A. M.; Shoichet, B. K. Docking for fragment inhibitors of AmpC beta-lactamase. *Proc. Natl. Acad. Sci. U. S. A.* **2009**, *106*, 7455–7460.
- (14) Chen, D.; Ranganathan, A.; Ijzerman, A. P.; Siegal, G.; Carlsson, J. Complementarity between in silico and biophysical screening approaches in fragment-based lead discovery against the A(2A) adenosine receptor. *J. Chem. Inf. Model.* **2013**, *53*, 2701–2714.
- (15) de Graaf, C.; Kooistra, A. J.; Vischer, H. F.; Katritch, V.; Kuijter, M.; Shiroishi, M.; Iwata, S.; Shimamura, T.; Stevens, R. C.; de Esch, I. J.; Leurs, R. Crystal structure-based virtual screening for fragment-like ligands of the human histamine H(1) receptor. *J. Med. Chem.* **2011**, *54*, 8195–8206.
- (16) Istyastono, E. P.; Kooistra, A. J.; Vischer, H.; Kuijter, M.; Roumen, L.; Nijmeijer, S.; Smits, R.; de Esch, I.; Leurs, R.; de Graaf, C. Structure-Based Virtual Screening for Fragment-Like Ligands of the G Protein-Coupled Histamine H4 Receptor. *MedChemComm* **2015**, *6*, 1003–1017.
- (17) Vass, M.; Schmidt, E.; Horti, F.; Keseru, G. M. Virtual fragment screening on GPCRs: a case study on dopamine D3 and histamine H4 receptors. *Eur. J. Med. Chem.* **2014**, *77*, 38–46.
- (18) Jacobson, K. A.; Gao, Z.-G. Adenosine receptors as therapeutic targets. *Nat. Rev. Drug Discovery* **2006**, *5*, 247–264.
- (19) Chen, J. F.; Eltzhig, H. K.; Fredholm, B. B. Adenosine receptors as drug targets—what are the challenges? *Nat. Rev. Drug Discovery* **2013**, *12*, 265–286.
- (20) Yang, Z.; Cerniway, R. J.; Byford, A. M.; Berr, S. S.; French, B. A.; Matherne, G. P. Cardiac overexpression of A1-adenosine receptor protects intact mice against myocardial infarction. *Am. J. Physiol Heart Circ Physiol* **2002**, *282*, H949–955.
- (21) Liu, W.; Chun, E.; Thompson, A. A.; Chubukov, P.; Xu, F.; Katritch, V.; Han, G. W.; Roth, C. B.; Heitman, L. H.; Ijzerman, A. P.; Cherezov, V.; Stevens, R. C. Structural basis for allosteric regulation of GPCRs by sodium ions. *Science* **2012**, *337*, 232–236.
- (22) Carlsson, J.; Coleman, R. G.; Setola, V.; Irwin, J. J.; Fan, H.; Schlessinger, A.; Sali, A.; Roth, B. L.; Shoichet, B. K. Ligand discovery from a dopamine D3 receptor homology model and crystal structure. *Nat. Chem. Biol.* **2011**, *7*, 769–778.
- (23) Katritch, V.; Kufareva, I.; Abagyan, R. Structure based prediction of subtype-selectivity for adenosine receptor antagonists. *Neuropharmacology* **2011**, *60*, 108–115.
- (24) Shen, M. Y.; Sali, A. Statistical potential for assessment and prediction of protein structures. *Protein Sci.* **2006**, *15*, 2507–2524.
- (25) Mysinger, M. M.; Carchia, M.; Irwin, J. J.; Shoichet, B. K. Directory of useful decoys, enhanced (DUD-E): better ligands and decoys for better benchmarking. *J. Med. Chem.* **2012**, *55*, 6582–6594.
- (26) Lorber, D. M.; Shoichet, B. K. Hierarchical docking of databases of multiple ligand conformations. *Curr. Top. Med. Chem.* **2005**, *5*, 739–749.
- (27) Mysinger, M. M.; Shoichet, B. K. Rapid context-dependent ligand desolvation in molecular docking. *J. Chem. Inf. Model.* **2010**, *50*, 1561–1573.
- (28) Ballesteros, J. A.; Weinstein, H. *Integrated Methods for the Construction of Three Dimensional Models and Computational Probing of Structure–Function Relations in G-Protein Coupled Receptors*; Academic Press: San Diego, 1995; pp 366–428.
- (29) Irwin, J. J.; Sterling, T.; Mysinger, M. M.; Bolstad, E. S.; Coleman, R. G. ZINC - A free tool to discover chemistry for biology. *J. Chem. Inf. Model.* **2012**, *52*, 1757–1768.
- (30) Mysinger, M. M.; Weiss, D. R.; Ziarek, J. J.; Gravel, S.; Doak, A. K.; Karpiak, J.; Heveker, N.; Shoichet, B. K.; Volkman, B. F. Structure-based ligand discovery for the protein-protein interface of chemokine receptor CXCR4. *Proc. Natl. Acad. Sci. U. S. A.* **2012**, *109*, 5517–5522.
- (31) Baell, J. B.; Holloway, G. A. New substructure filters for removal of pan assay interference compounds (PAINS) from screening libraries and for their exclusion in bioassays. *J. Med. Chem.* **2010**, *53*, 2719–2740.
- (32) Hopkins, A. L.; Keseru, G. M.; Leeson, P. D.; Rees, D. C.; Reynolds, C. H. The role of ligand efficiency metrics in drug discovery. *Nat. Rev. Drug Discovery* **2014**, *13*, 105–121.
- (33) Wawer, M.; Bajorath, J. Similarity-potency trees: a method to search for SAR information in compound data sets and derive SAR rules. *J. Chem. Inf. Model.* **2010**, *50*, 1395–1409.
- (34) Jung, K. Y.; Kim, S. K.; Gao, Z. G.; Gross, A. S.; Melman, N.; Jacobson, K. A.; Kim, Y. C. Structure-activity relationships of thiazole and thiadiazole derivatives as potent and selective human adenosine A3 receptor antagonists. *Bioorg. Med. Chem.* **2004**, *12*, 613–623.
- (35) van Muijlwijk-Koezen, J. E.; Timmerman, H.; Vollinga, R. C.; Kunzel, J. F. v. D.; de Groot, M.; Visser, S.; Ijzerman, A. P. Thiazole and thiadiazole analogues as a novel class of adenosine receptor antagonists. *J. Med. Chem.* **2001**, *44*, 749–762.
- (36) van Tilburg, E. W.; van der Klein, P. A.; de Groot, M.; Beukers, M. W.; Ijzerman, A. P. Substituted 4-phenyl-2-(phenylcarboxamido)-1,3-thiazole derivatives as antagonists for the adenosine A(1) receptor. *Bioorg. Med. Chem. Lett.* **2001**, *11*, 2017–2019.
- (37) Baraldi, P. G.; Cacciari, B.; Moro, S.; Spalluto, G.; Pastorin, G.; Da Ros, T.; Klotz, K. N.; Varani, K.; Gessi, S.; Borea, P. A. Synthesis, biological activity, and molecular modeling investigation of new pyrazolo[4,3-e]-1,2,4-triazolo[1,5-c]pyrimidine derivatives as human A(3) adenosine receptor antagonists. *J. Med. Chem.* **2002**, *45*, 770–780.
- (38) Rodriguez, D.; Gao, Z. G.; Moss, S. M.; Jacobson, K. A.; Carlsson, J. Molecular Docking Screening Using Agonist-Bound GPCR Structures: Probing the A2A Adenosine Receptor. *J. Chem. Inf. Model.* **2015**, *55*, 550–563.

- (39) Carlsson, J.; Yoo, L.; Gao, Z.-G.; Irwin, J. J.; Shoichet, B. K.; Jacobson, K. A. Structure-based discovery of A2A adenosine receptor ligands. *J. Med. Chem.* **2010**, *53*, 3748–3755.
- (40) Barelier, S.; Eidam, O.; Fish, I.; Hollander, J.; Figaroa, F.; Nachane, R.; Irwin, J. J.; Shoichet, B. K.; Siegal, G. Increasing chemical space coverage by combining empirical and computational fragment screens. *ACS Chem. Biol.* **2014**, *9*, 1528–1535.
- (41) Kooistra, A. J.; Roumen, L.; Leurs, R.; de Esch, I. J.; de Graaf, C. From heptahelical bundle to hits from the Haystack: structure-based virtual screening for GPCR ligands. *Methods Enzymol.* **2013**, *522*, 279–336.
- (42) Kolb, P.; Phan, K.; Gao, Z. G.; Marko, A. C.; Sali, A.; Jacobson, K. A. Limits of ligand selectivity from docking to models: in silico screening for A(1) adenosine receptor antagonists. *PLoS One* **2012**, *7*, e49910.
- (43) Rodríguez, D.; Brea, J.; Loza, M. I.; Carlsson, J. Structure-based Discovery of Selective Serotonin 5-HT1B Ligands. *Structure* **2014**, *22*, 1140–1151.
- (44) Totrov, M.; Abagyan, R. Flexible ligand docking to multiple receptor conformations: a practical alternative. *Curr. Opin. Struct. Biol.* **2008**, *18*, 178–184.
- (45) Katritch, V.; Jaakola, V. P.; Lane, J. R.; Lin, J.; Ijzerman, A. P.; Yeager, M.; Kufareva, I.; Stevens, R. C.; Abagyan, R. Structure-based discovery of novel chemotypes for adenosine A(2A) receptor antagonists. *J. Med. Chem.* **2010**, *53*, 1799–1809.
- (46) Mason, J. S.; Bortolato, A.; Congreve, M.; Marshall, F. H. New insights from structural biology into the druggability of G protein-coupled receptors. *Trends Pharmacol. Sci.* **2012**, *33*, 249–260.
- (47) Congreve, M.; Andrews, S. P.; Dore, A. S.; Hollenstein, K.; Hurrell, E.; Langmead, C. J.; Mason, J. S.; Ng, I. W.; Tehan, B.; Zhukov, A.; Weir, M.; Marshall, F. H. Discovery of 1,2,4-triazine derivatives as adenosine A(2A) antagonists using structure based drug design. *J. Med. Chem.* **2012**, *55*, 1898–1903.
- (48) Gaulton, A.; Bellis, L. J.; Bento, A. P.; Chambers, J.; Davies, M.; Hersey, A.; Light, Y.; McGlinchey, S.; Michalovich, D.; Al-Lazikani, B.; Overington, J. P. ChEMBL: a large-scale bioactivity database for drug discovery. *Nucleic Acids Res.* **2012**, *40*, D1100–1107.
- (49) Bamborough, P.; Brown, M. J.; Christopher, J. A.; Chung, C. W.; Mellor, G. W. Selectivity of kinase inhibitor fragments. *J. Med. Chem.* **2011**, *54*, 5131–5143.
- (50) Babaoglu, K.; Shoichet, B. K. Deconstructing fragment-based inhibitor discovery. *Nat. Chem. Biol.* **2006**, *2*, 720–723.
- (51) Pei, J.; Kim, B. H.; Grishin, N. V. PROMALS3D: a tool for multiple protein sequence and structure alignments. *Nucleic Acids Res.* **2008**, *36*, 2295–2300.
- (52) Sali, A.; Blundell, T. L. Comparative protein modelling by satisfaction of spatial restraints. *J. Mol. Biol.* **1993**, *234*, 779–815.
- (53) Shoichet, B. K.; Kuntz, I. D. Matching chemistry and shape in molecular docking. *Protein Eng., Des. Sel.* **1993**, *6*, 723–732.
- (54) Nicholls, A.; Honig, B. A rapid finite difference algorithm, utilizing successive over-relaxation to solve the Poisson–Boltzmann equation. *J. Comput. Chem.* **1991**, *12*, 435–445.
- (55) Weiner, S. J.; Kollman, P. A.; Case, D. A.; Singh, U. C.; Ghio, C.; Alagona, G.; Profeta, S.; Weiner, P. A new force field for molecular mechanical simulation of nucleic acids and proteins. *J. Am. Chem. Soc.* **1984**, *106*, 765–784.
- (56) JChem, version 5.11.4; ChemAxon: Budapest, 2012.
- (57) Cordeaux, Y.; Briddon, S. J.; Megson, A. E.; McDonnell, J.; Dickenson, J. M.; Hill, S. J. Influence of receptor number on functional responses elicited by agonists acting at the human adenosine A(1) receptor: evidence for signaling pathway-dependent changes in agonist potency and relative intrinsic activity. *Mol. Pharmacol.* **2000**, *58*, 1075–1084.
- (58) Vernall, A. J.; Stoddart, L. A.; Briddon, S. J.; Hill, S. J.; Kellam, B. Highly potent and selective fluorescent antagonists of the human adenosine A(3) receptor based on the 1,2,4-triazolo[4,3-a]quinoxalin-1-one scaffold. *J. Med. Chem.* **2012**, *55*, 1771–1782.
- (59) Stoddart, L. A.; Kellam, B.; Briddon, S. J.; Hill, S. J. Effect of a toggle switch mutation in TM6 of the human adenosine A(3) receptor on Gi protein-dependent signalling and Gi-independent receptor internalization. *Br. J. Pharmacol.* **2014**, *171*, 3827–3844.
- (60) Areias, F.; Costa, M.; Castro, M.; Brea, J.; Gregori-Puigjane, E.; Proenca, M. F.; Mestres, J.; Loza, M. I. New chromene scaffolds for adenosine A(2A) receptors: synthesis, pharmacology and structure-activity relationships. *Eur. J. Med. Chem.* **2012**, *54*, 303–310.